
Measuring Regional Lung Function Using Oxygen-Enhanced MRI

A dissertation submitted in partial fulfillment of the requirements for the
degree of Bachelor of Technology (Honors) in Medical Physics and Imaging
Technology

Alex Jin

ID: 6841775

Supervisor: Beau Pontré & Kelly Burrowes

Department of Physics, 2017

Contents

| | |
|---|-----------|
| 1 Abstract | 3 |
| 2 Introduction | 3 |
| 3 Theory | 5 |
| 3.1 Basic Magnetic Resonance Physics | 5 |
| 3.2 MR Signal - T1 Relaxation | 6 |
| 3.3 Project Focus | 7 |
| 4 Methods | 9 |
| 4.1 Image Preparations | 9 |
| 4.1.1 Equipment | 9 |
| 4.2 Pulse Sequence | 10 |
| 4.3 Image acquisition and analysis - 1.5T MRI | 10 |
| 4.3.1 Image acquisition | 10 |
| 4.3.2 Experiment Optimisation and implementation | 12 |
| 4.3.3 Data analysis - ROI selection | 13 |
| 4.3.4 Quality Control | 13 |
| 4.3.5 Regional Distribution of Specific Ventilation | 14 |
| 4.4 Image acquisition and analysis - 3T MRI | 14 |
| 5 Results | 15 |
| 5.1 Results and analysis - 1.5T | 15 |
| 5.1.1 Behavior of signal intensity following air - oxygen cycle | 15 |
| 5.1.2 Thresholding blood | 15 |
| 5.1.3 Comparative Post-Threshold Data Analysis | 16 |
| 5.2 Shared Data - Data Analysis and Quantification | 16 |
| 5.2.1 Results and Analysis - 3T | 19 |
| 6 Discussion | 20 |
| 6.1 Analysis of 1.5T experiments | 20 |
| 6.1.1 Thresholding of blood | 21 |
| 6.1.2 Post-Threshold analysis | 22 |
| 6.2 Shared Data analysis | 23 |
| 6.2.1 Quantifying limitations in our experiment | 23 |
| 6.3 Analysis of 3T experiments | 24 |

| | |
|---------------------|-----------|
| 7 Conclusion | 25 |
| 8 Reference | 26 |

1 Abstract

Non-invasive and non-radiative imaging techniques such as MRI encourage us to explore new ways in delivering reliable diagnostic information. Specific ventilation (SV) within lungs been previously measured in experiments such as Multiple Breath Washouts (MBW) and inhalation of radioactive molecules. While tracer inspiratory experiments yield spatial information, SV is consistent throughout both experiments. The disadvantage is that inhalation of radioactive isotopes limit repeatability of clinical imaging. Using an fMRI approach, both SV and spatial information of SV can be obtained safely. Single sagittal slice of the right lung were imaged 220 times switching the air delivery from room air to 100% oxygen every 20 breaths. Percentage of oxygen entering the lungs following inhalation change MR signal intensity of lungs. The MR signal changes when switching from air to 100% oxygen due to paramagnetic properties of oxygen. To acquire lung images showing true signals from oxygen, a requirement of a non-selective inversion pulse before the HASTE sequence is needed. Without the non-selective inversion, image will present signals coming from large blood vessels affecting further data-analysis.

2 Introduction

Respiration describes the exchange of gas in our respiratory tract. The pressure inside the intrapulmonary cavity has the same atmospheric pressure of air at 760mmHg. During inspiration, the diaphragm begins to contract increasing volume inside the lung cavity; as volume increases, pressure decreases. Due to the pressure gradient, the gas travels through our respiratory tract, into the lungs, balancing out the pressure difference [16]. Vice versa, during expiration, the diaphragm relaxes and returns intrapulmonary pressure to normal. From opposite pressure gradients, air is expired out resulting in normal pressure balances. Gas exchange occurs from the interaction of capillaries and small air sacs called the alveoli located in the alveoli walls. The walls of alveoli share the same membrane as capillaries where oxygen and carbon dioxide exchange occur as we breath in and out [16].

Respiratory diseases impact the lungs ability for regular gas exchange due to defects in ventilation and/or perfusion. Any defect in normal respiratory function may indicate prevalence of interstitial lung disease such as Idiopathic Pulmonary Fibrosis. Respiratory disease

account for at least 14% of deaths worldwide and trends suggest its occurrence is increasing [1]. In New Zealand alone, Chronic Obstructive Pulmonary Disease (COPD) is estimated to be present in 15% of adults age 45 years and over. COPD is the 4th leading cause of death in New Zealand while costing upwards of \$192 million in health care costs every year [2].

Specific ventilation (SV) describes the ratio of inspired gas divided by the end expiratory volume of lung. SV defines the efficiency of lung in exchanging inspired air and may be a precursor to most respiratory disease [15]. Measurement of regional specific ventilation (SV) have previously been obtained using imaging modalities such as Computed Tomography (CT) and nuclear medicine using ionising isotopes as contrast agents [9, 10, 13, 14, 15]. A new technique has been developed in determining SV using oxygen-enhanced proton MRI, greatly reducing harmful effects such as exposure to radiation which allows for increased repeatability [4, 6, 13, 14, 15].

SV can be measured using Oxygen-enhanced MRI [3, 14, 15]. Clear anatomical images of the lung remain difficult from the lack of tissue available in the lung cavity. Proton enhanced MRI map oxygen concentrations in each voxel correlating to its voxel brightness. Voxels presenting high oxygen concentration show brighter and low concentrations darker. Inhalng different concentrations of oxygen will show contrast in signal intensity relative to each voxel of lung based on voxel oxygen concentration. Using pre-written algorithms, oxygen concentration is directly related to a SV unit in the same voxel.

In experimental conditions, delivery of flow can be manually switched from air to 100% oxygen using a switching valve. Scanning subjects breathing in room air then switching to 100% oxygen some acquisitions later, plots of mean signal intensity of lung ROI for each image can be obtained which gives a graphical representation of SV. Due to low oxygen concentrations in air (21%), mean signal intensities of lung following inhalation of room air will show lower MR signals compared to images acquired after inhalation of 100% oxygen. After the switch from air to oxygen, mean MR signal will rise in successive images until reaching a new equilibrium. Measure of SV is quantified based on measuring half the rise time of reaching new equilibrium [15].

In this project, we have explored the background and applicability of this technique in modern day medicine. Quantification of specific ventilation will be explained focusing on the significance of the change in longitudinal (T1) relaxation time from measured signals [14, 15]. Image analysis will be explored in depth exploring how we can quantify a measure of SV from images of subject lungs. Lastly, I will explain the results and how this technique

was able to validate the known vertical distribution of SV in lungs [8, 12, 14] and limitations seen with this SVI technique.

3 Theory

3.1 Basic Magnetic Resonance Physics

Nuclear magnetic resonance is the foundation of MRI. Atoms that have odd numbers of protons or neutrons like hydrogen (1 proton) will display an intrinsic magnetic moment and angular momentum. In normal conditions these magnetic moments are in random configuration cancelling each other out resulting in zero net magnetization. When a strong external magnetic field (B_0) is applied, the magnetic moments in proximity align parallel or anti-parallel to B_0 [18]. Magnetic moments in parallel with B_0 is said to be at a low energy state and when anti-parallel, it is at a high-energy state. When atoms are aligned, the net magnetization vector [18, 19] along the longitudinal direction increases to an equilibrium state, represented by vector M_0 . In MRI, the manipulation of NMV by process of radiofrequency (RF) excitation allows detection of changes in signal intensities through varying relaxation times, later transformed into images applying complex math algorithms [15].

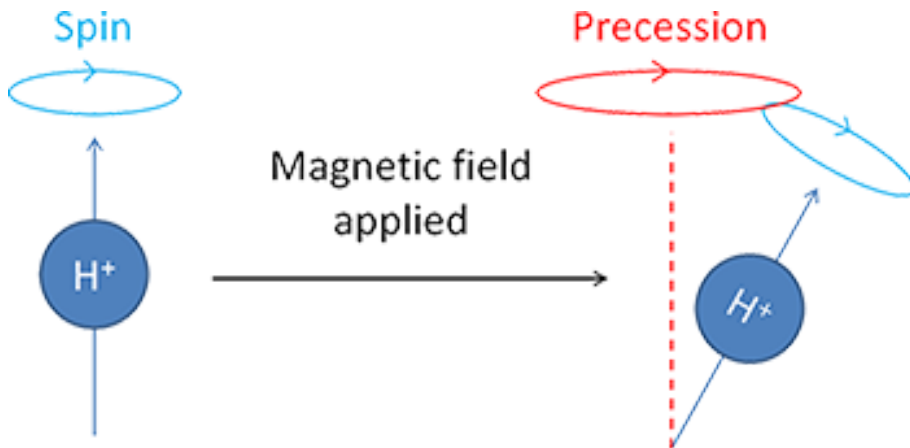


Figure 1: Hydrogen atom at rest on left; Hydrogen atom precessing after application of external magnetic field on right [20].

At rest, the NMV is in direction of the longitudinal (z) plane, parallel to B_0 and depends only on longitudinal (M_z) magnetizations. When B_0 is applied, protons align and precess about B_0 . The ratio of atoms precessing parallel or anti-parallel to B_0 when only B_0 is present is the equilibrium NMV. The precession rate is also known as the Lamor frequency and is

fundamental to MRI [17]. Hydrogen atoms for example precess at the Lamor frequency of 42MHz/T[17]. When we apply a radio-frequency pulse (RF) at 1T, the RF pulse is tuned to 42MHz matching the precession rate of hydrogen causing a phenomenon called resonance. Resonance is when energy is transferred between same precessing frequencies (i.e hydrogen atoms and the applied magnetic field) causing an amplification of signal that decays over time; this is known as the free induction decay (FID) and is the observed signal following RF excitation [18, 19].

RF coils can both excite and detect signals following excitation. When an RF pulse is applied, precessing atoms are flipped into a higher energy state where they will relax to give off a detectable signal. An RF pulse flips the NMV into the transverse plane. The NMV faces direction of the transverse plane as M_z decreases to zero and Mt increases to a new equilibrium [18, 19]. Following the excitation, the NMV will relax back to its equilibrium in the longitudinal direction as Mt decreases and M_z increases to equilibrium. This is known as T1 relaxation and is fundamental in determining oxygen concentration in each voxel of lung.

3.2 MR Signal - T1 Relaxation

Differentiation of tissue types is possible by analysing different signals measured following RF excitation. Different tissue types have different relaxation times which is empirical in providing contrast for acquired images. This contrast depends on the time taken for the signal to relax back to equilibrium following RF excitation and is given by two types of relaxation; longitudinal (T1) and transverse (T2) relaxation [18].

T1 relaxation describes the time taken for the NMV to relax back into the longitudinal plane following RF excitation. T1 relaxation describes the transfer of energy from spins to its surrounding lattice as it equilibrates to its original energy state [18]. Different tissues transfer energy at different rates depending on the complexity of lattice. Oxygen is largely paramagnetic and influence T1 relaxation times depending on its concentration [15]. An oxygen dense voxel will exhibit faster T1 relaxation compared with voxels having lower oxygen concentrations [15]. It is possible to map change in oxygen concentration relative to each voxel of tissue depending on relaxation times. For example, a normal lung image filled with room air containing 21% oxygen will present a normal lung image. Switching the flow rate to 100% oxygen, the difference in percentage oxygen inhalation will alter resulting T1 relaxation time of each voxels. Signal inside the lung cavity will appear slightly brighter compared air filled lungs due to do the increase in percentage oxygen uptake [15]. Conversely, switching

flow delivery to room air, following images will show gradual decrease in MR signal as less oxygen is getting exchanged.

3.3 Project Focus

Because the lung has an empty cavity, acquired image show lack of signal from limited tissue available. New developments in Oxygen MRI provide accurate measurements in lung tissue using Oxygen as a contrast agent. Oxygen is a paramagnetic molecule that interacts with the applied field from a MRI scanner providing contrast for analysis. By delivering larger concentrations of oxygen to lungs, a rise in mean signal is observed, sufficient to use as a contrast agent. Specifically, imaging a volunteer breathing room air versus the volunteer breathing 100% oxygen will provide different signal intensities which we later use to quantify SV.

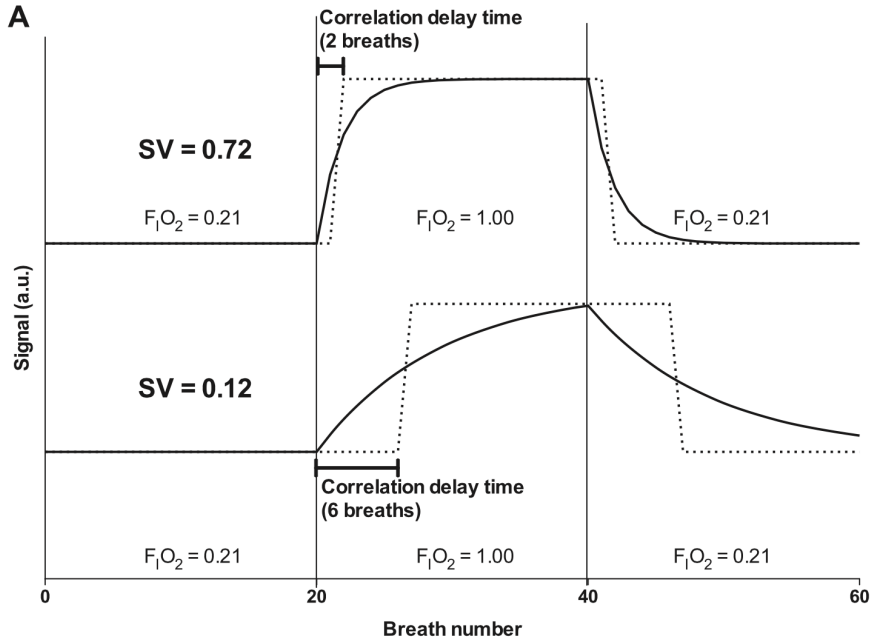


Figure 2: Plot of signal intensity versus the number of breath for a single voxel of lung unit presenting SV values of 0.72 and 0.12. As gas delivery is switched from air to oxygen, clear rise in signal is observed to its new threshold. Lung units presenting higher SV show faster rise times vs low lung SV units [15].

Like Figure 2, we expect to see a rise in signal as we switch the oxygen delivery from room air to 100% oxygen. More oxygen to the lungs will increase signal inside the lung cavity. The increasing signal will reach a new equilibrium threshold until gas delivery is switched to room

air where it will decrease back to its previous equilibrium threshold.

Correlation delay time is introduced as the number of breathes needed to reach half the rise time of the equilibrium curve[15]. Lung units given by a dimensionless quantity, describes the efficiency of gas exchange in one ventilation unit or voxel. Lung units with higher SV equilibrate much faster than lung units of lower SV. Therefore, higher SV lung units (e.g. $SV = 0.72$), the correlation delay time is 2 breathes, showing the high efficiency of the lungs ability to exchange gas. Vice versa, a lower lung unit presenting a SV of 0.12 will show a longer correlation delay time (6 breathes) showing inefficient gas exchange.

Units with higher specific ventilation equilibrate much faster compared to units with lower SV. The related correlation delay time shows to be much shorter in higher SV (2 – 4 breaths) compared to lower SV units (6 – 10 breaths). Lung units above SV of 0.5 show little difference in correlation delay. This is because equilibration for these high SV units happen too fast; a correlation delay time of under 1 breath – hence not resolvable. This is expected from the basis of previous studies. Very few lung units present SV higher than 0.5 [8,14, 15]; presence of lung disease is usually associated with units presenting reduced SV. Based on this information, this limitation is of minor significance [8, 14, 15].

Correlations have been found with delay time and SV by previous studies [15]. By translating correlation delay times to values of SV in the lung area, an SV map can be produced showing the relative SV at each voxel (figure 3).

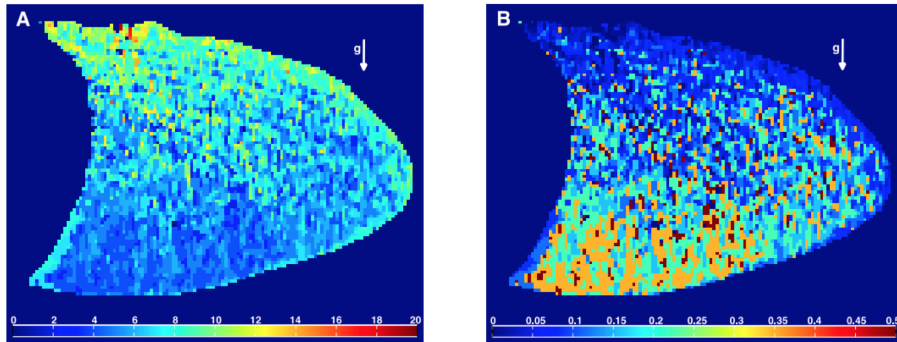


Figure 3: Lung map of correlation delay time (a) and corresponding regional SVI Map of same lung. Lung units near the zero height show faster correlation delay times directly relating to higher SV units [15].

4 Methods

This project consisted of three main sections:

- Experimental preparations; ordering and 3D printing necessary equipment, code optimisation and data analysis of shared images from San Diego and Sydney groups.
- Image acquisition and analysis using 1.5T MRI.
- Image acquisition and analysis using 3T MRI.



Figure 4: Schematic summarising steps taken during the project

4.1 Image Preparations

4.1.1 Equipment

Switching gas delivery to subjects being scanned is made possible using a switching valve located outside the MRI scanning room connected to plastic tubing that is attached to a 3D-printed bypass flow attachment [17] shown on figure 5. The bypass flow attachment is connected to a Hans Rudolph face-mask (Hans Rudolph, dead space 73ml -113ml) [17].

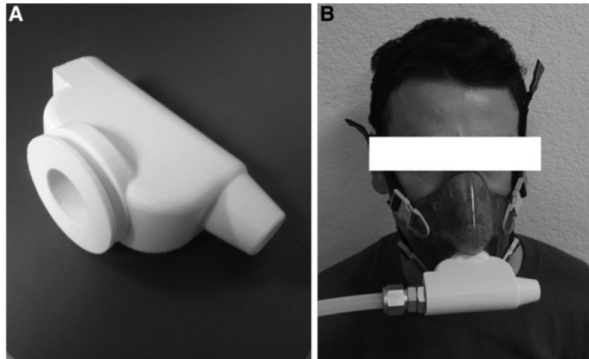


Figure 5: 3D-Printed flow attachment (A); Hans Rudolph Face-mask attached with flow attachment (B) [17]

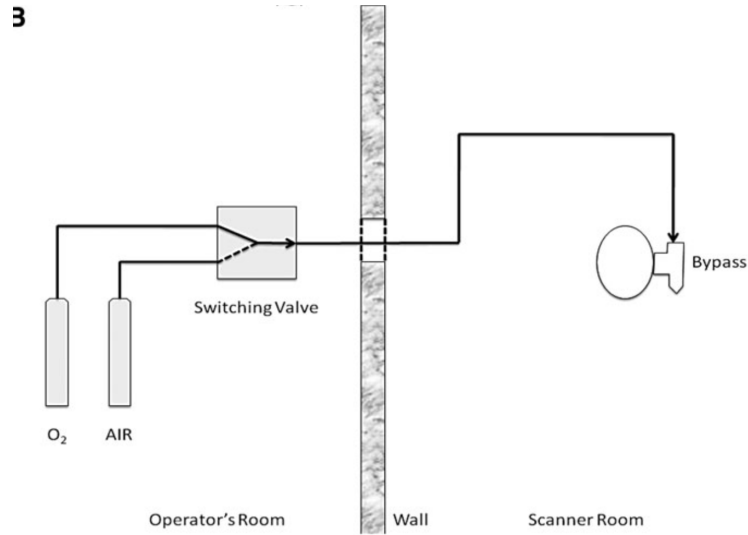


Figure 6: Schematic of experimental set up showing switching valve outside scanner room [17].

4.2 Pulse Sequence

All images were acquired using a slice-selective, inversion recovery ($T_1=1100\text{ms}$) single-shot fast spin echo (SSFSE) pulse sequence, implementing the half- Fourier single-shot turbo spin echo (HASTE) acquisition. The field of view was set to $40\times 40\text{cm}$, echo time of 30ms , 15mm of slice thickness.

The slice selective inversion pulse acts to null blood signals in the imaged lung slice and not the whole lung leading to a major limitation in any further analysis. Shared images of lungs showing no signal from blood were acquired using a non-selective inversion pulse sequence where it does not use a slice selective gradient at the time of RF excitation. The pulse diagrams are shown on figure 7/8.

4.3 Image acquisition and analysis - 1.5T MRI

4.3.1 Image acquisition

Replicating methods proposed by Sa et al [15] acquiring a total of 220 images split into 5 blocks of air and oxygen. Volunteers are asked to take a normal breath in and out, back to their estimated functional residual capacity (FRC) in a period of 6 seconds. On the 6th second, the MRI scanner makes a loud clicking sound indicating the volunteer to repeat the breath hold task, aiming to attain the same FRC as the previous image. Emphasis on attaining the same FRC at each time of image acquisition is asked to acquire clean sets of data

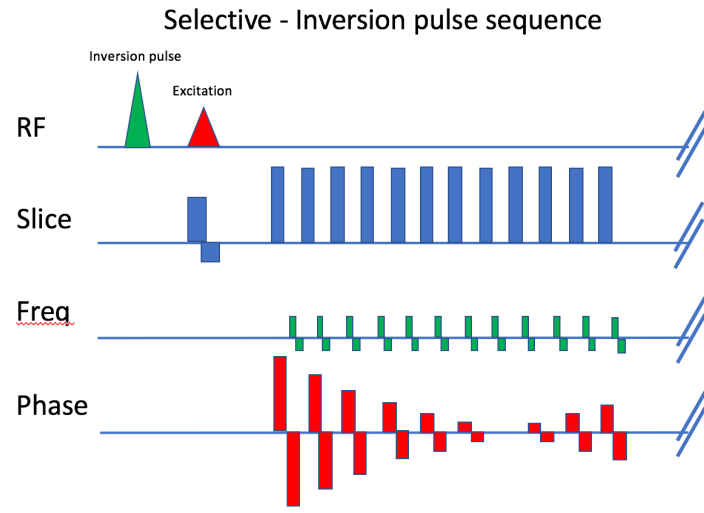


Figure 7: Slice-selective inversion pulse sequence: Inversion pulse at the start with a gradient slice selection frequency at second RF excitation

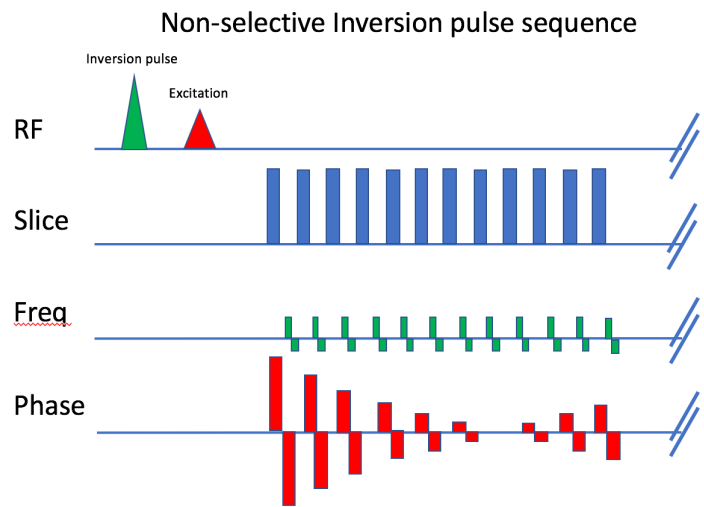


Figure 8: non-selective inversion pulse sequence: Inversion pulse at the start with a gradient slice selection frequency at second RF excitation

where little lung volume variation is seen.

Each block refers to an air – oxygen cycle consisting of 20 images when volunteer breathes in air (21%) and another 20 breathing oxygen (100%). To switch air delivery from room air to oxygen, a face mask and switching valve is required. It is essential for the flow delivery to switch correctly from air to oxygen to ensure reliable measurements.

Volunteers were laid in a supine posture wearing a face-mask (Hans Rudolph, dead space 73ml -113ml) connected to a 3D-printed bypass flow attachment. The bypass flow attachment allows for rapid switching from inspiration of air (21%) to oxygen (100%). The flow attachment is connected to a tube that connects the switching valve outside the scanner room where switching of inspired air-oxygen is controlled manually. Subjects were trained to gate their breathing consistently following a sound heard from the MRI scanner before being imaged. After a sound is heard, the subject takes a normal tidal breath in and breathe out back to functional residual capacity within a 6 second period where each image is acquired. Specifically, images were acquired during the post-expiratory pause at FRC which gave consistency in lung volume observed from the images.

4.3.2 Experiment Optimisation and implementation

Normal experimental procedure of acquiring 220 images was performed on a 1.5T scanner. The breathing interval between images was set to 5 seconds and ran test scans to see if the 5 second interval gave sufficient time to breath in and out followed by a breath hold. After the test scans, the experiment was carried out imaging 5 blocks of air-oxygen intervals.

We started our scan with an experiment to make sure our oxygen delivery system was working when switching from air to oxygen. The breathing interval was changed to 6 seconds as the previous 5 second interval was too fast for normal breathing rates. We first imaged our volunteer breathing normal air for 10 images followed by 30 images breathing 100% oxygen. As we are using oxygen as our contrast agent, we expect to see an increase in mean signal intensity inside the lung when our volunteer breathes in 100% oxygen. The 30 images at oxygen ensures the signal has equilibrated after the 30 images. We then carried on with our normal experiment acquiring the total of 220 images.

4.3.3 Data analysis - ROI selection

Using a prewritten MATLAB code, manual ROI selection is possible for each image in series [15]. The code loads an image onto a user interface which allows for manual ROI selection to be used in further analysis. An ROI is chosen by using multiple nodal points to outline the region of lung shown by the blue tracing line on figure 1. The manually selected ROI becomes the reference ROI of the whole image series and becomes the lung ROI mask. Essentially, all images in the series is a deformation of each other due to movement of the lung. An ROI needs to be manually selected for each of the 220 images in the series for the best results in our final analysis where we quantify SV. By selecting individual ROI's for each image allows us to perform a quality check for the series.

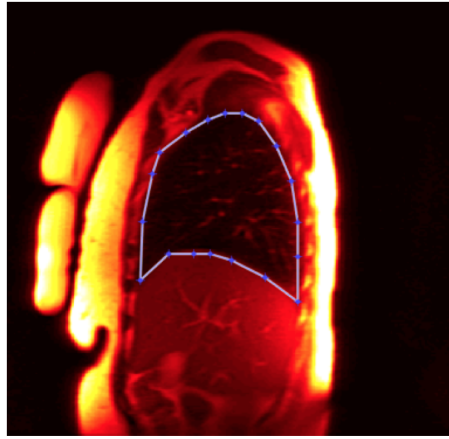


Figure 9: Custom graphical user interface with ROI selection. Blue tracers with square nodal points trace outline of lung

The lung ROI mask is important in further analysis. As all further data analysis comes from this ROI, it is important to make it as accurate as possible.

4.3.4 Quality Control

Not all images in the 220 image series will be available to use for final analysis. The lung volume of multiple image in series may vary too much compared to the reference ROI and needs to be discarded or replaced with interpolated images from its neighbours to provide a clean series of images.

Quality control of the acquired images was performed individually. Image rejection was determined on visual inspection of the acquired image series. By comparing images showing a visual difference in volume to a reference ROI, we determine if an image is reliable for

use. If an image showed 10% or greater change in volume compared to the reference ROI, the image is rejected and replaced by an interpolated image from neighboring images. For clean data sets acquired using the non-selective inversion pulse, around 4.3% of images in the series failed to meet the quality criteria and was rejected. Discarding images presenting large volume change was achieved by counting the pixels of each unique ROI. By comparing percentage change in volume, image presenting large percentage volume change were discarded and replaced.

Most images acquired by us did not go through the usual quality control inspection as most images presented large amounts of blood signal and other methods such as thresholding was introduced.

4.3.5 Regional Distribution of Specific Ventilation

From outputs of pre-written MATLAB codes, regional distribution of SV is shown in the whole lung as well as quantified values of SV at each height of lung. The trends and observed distributions will be discussed in later sections of this report.

4.4 Image acquisition and analysis - 3T MRI

Due to blood signals showing up in our image acquisitions, a 3T scanner was used in hope to cancel out these blood signals.

Image acquisition using the 3T MRI scanner was performed using the same parameters and equipment as the 1.5T. Because inversion times vary in 3T and 1.5T scanners, multiple experiments finding the best inversion time for nulling blood signals was performed rather than experiments finding signal changes stepping through air - oxygen cycles.

In attempt to signal out the blood, multiple TI's (1000-1400ms) used in test scans where our volunteer followed the same breathing interval procedure as the 1.5T. We found no improvements in quality with the successive scans but carried on with our normal experiment of 220 images using a TI of 1300ms.

The second experiment consisted of another attempt in nulling signals created by large blood vessels in close proximity to the lungs. We imaged our volunteer performing the same breathhold procedure for 8 breaths at multiple TI's. We started with 8 images with a TI of 600ms and stepping through by 100ms to a final 8 images with TI at 2800ms. We wanted to

see if there was a TI that would totally null the signals from blood or find the optimal TI to use for our next scans.

5 Results

5.1 Results and analysis - 1.5T

Images acquired using the 1.5T scanner had showed blood signals bleeding through. Even after using an inversion pulse in attempt to null blood signal, most resulting images showed blood coming through during image acquisition at various signal intensity (figure 10b, c). Images unaffected by blood were rare and came in random intervals (figure 10a).

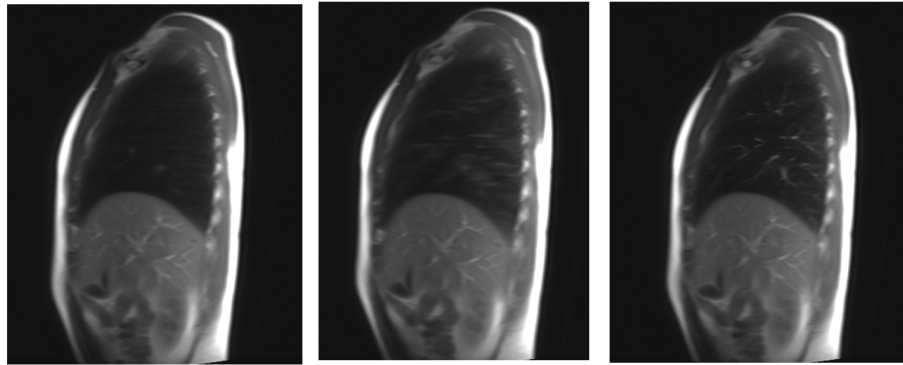


Figure 10: The leftmost picture shows a clean image unaffected by blood in the region of lung (mean intensity = 48)(A). 10B and 10C shows the different grade of blood signal contamination in our region of interest (mean intensity for 10b = 68; 10c = 81).

5.1.1 Behavior of signal intensity following air - oxygen cycle

To check our experiment was performing as it should with correct switching of air – oxygen delivery, mean signal intensities of individual images in series was analysed shown on figure 11. We expected to see lower signal intensities following inhalation of only air and a steady increase in signal intensity following inhalation of 100% oxygen. Vice versa, we should see the signal decrease when we switch back to air

5.1.2 Thresholding blood

Due to apparent blood signals present in acquired images, manual thresholding of blood signal inside the lung cavity was performed. Selecting only the ROI of lung and implementing a test compares voxel intensities with a set threshold value, thresholding of blood signals was

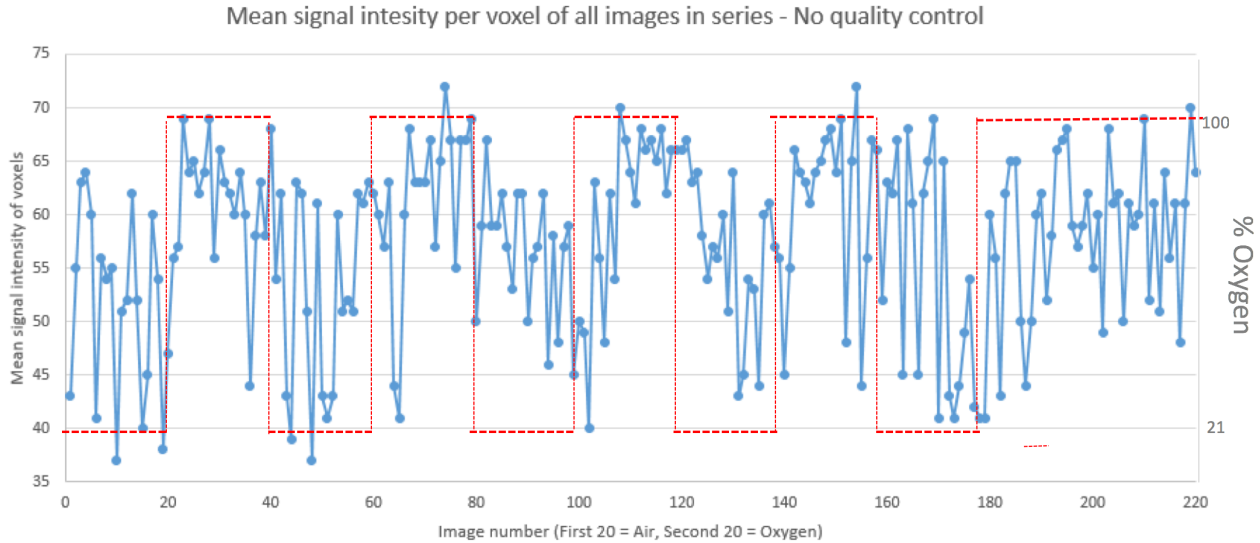


Figure 11: Plot showing mean signal intensity at each lung image ROI. Images between 0 – 20 were taken following inhalation of air (21%) and the next 20 images taken following inhalation of 100% Oxygen. Every 20 images, the oxygen delivery was switched alternating in air – oxygen cycles.

possible. The threshold value was set at multiple intensities (60,70 and 90) shown on figure 10a/b/c.

Looking at threshold results, the final threshold value of 70 was set. Clean images presenting no blood signal presented mean MR signal intensities ranging from 40 to high 60's. For this reason, any signal presenting higher values than 70 was regarded as noise and replaced by a 0 for further analysis.

5.1.3 Comparative Post-Threshold Data Analysis

A second plot of mean signal for each image in series was obtained using the thresholding lung images for comparison. As a result, a more noticeable trend is observed in figure 14.

5.2 Shared Data - Data Analysis and Quantification

Analysed data from pre to post-threshold show a clear correlation from clean images and images affected by blood. Using shared data of clean images and blood spoiled images, the effect of blood signal is further demonstrated.

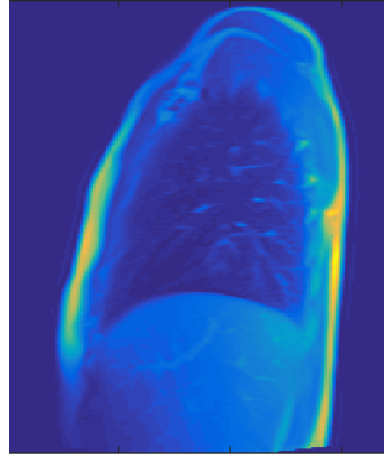


Figure 12: Lung image showing blood signal. Using different threshold values, I tried to find the best value that would null most blood signal while also giving reliable signal mean intensities.

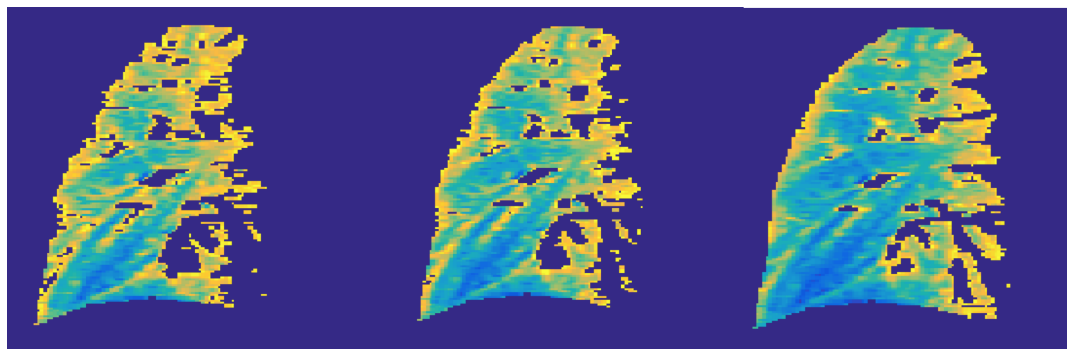


Figure 13: Post-threshold lung images with threshold value 60, 70 and 90 respectively. All values relative to the grey scale.

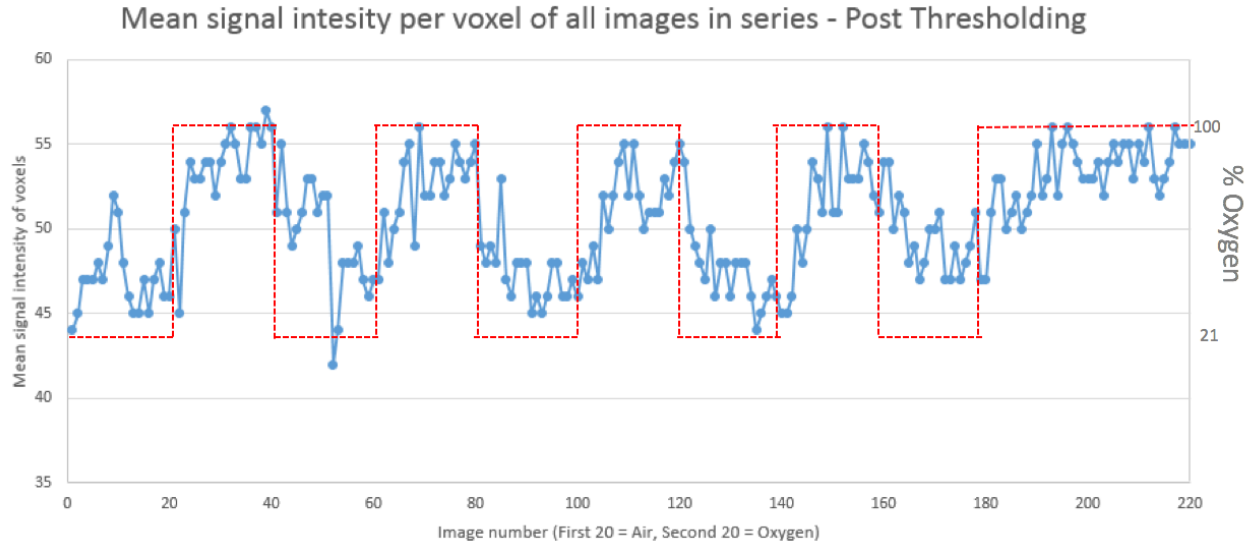


Figure 14: Plot showing mean signal intensity at each lung image ROI post threshold. This plot has much more observable trend compared to figure 11 where mean intensities gradually fluctuate up and down following inhalation of different percentage of oxygen.

The first set of shared data showed an image series following same experimental procedure measuring regional SV showed no apparent signal from blood. Performing the same analysis as before, regional SV maps and SV height plots were generated.

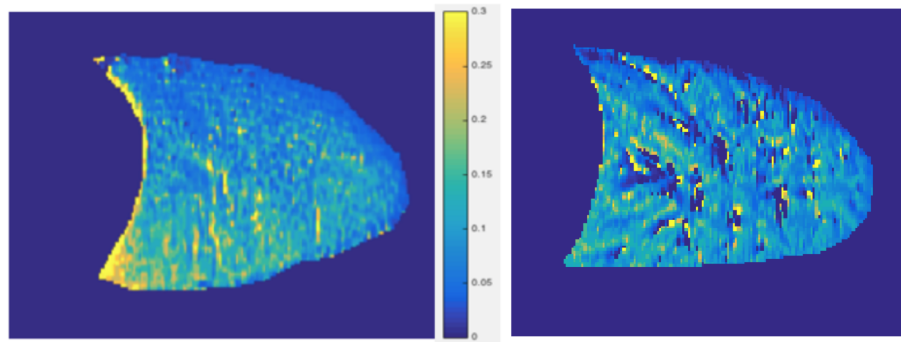


Figure 15: Regional SV distribution in lung ROI of clean image set vs blood spoiled image set. Brighter colours correlate to higher SV lung units in that region.

Distribution of SV clean image shows a uniform trend. Lung voxels at lower areas show more intense profiles compared to the top. On the blood spoiled SV map (right), there is no observable trend. Voxel intensities show to be spread out all across the lung rather than following some gradient.

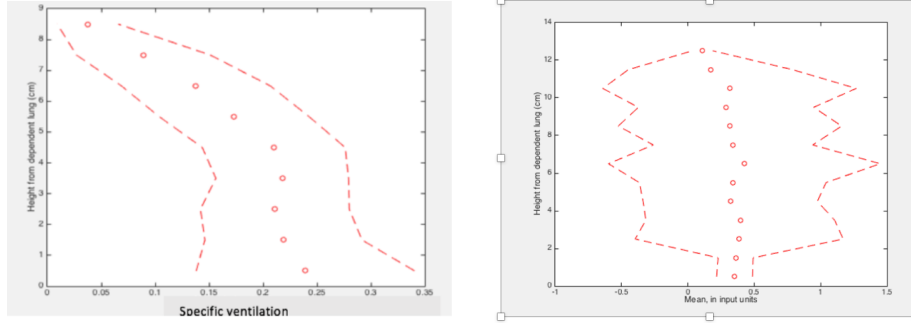


Figure 16: Plot presenting average SV in each centimeter height of lung. Image on left shows height plot of shared data showing no blood signal. Image on RIGHT show same height plot but for lungs presenting noise from blood.

The resulting height plots show a uniform distribution of SV per centimeter height of lung in clean images with no spikes and negative values on the x axis. Height plot of blood spoiled image show no observable trend and random spikes feeding into negative values.

5.2.1 Results and Analysis - 3T

Using multiple inversion times with the 3T scanner yielded no significant difference in image quality past an inversion time of 900ms. Images acquired using TI's of 600-800ms results in low quality image shown on fig 4a. Images acquired using a TI of 1300ms (fig 4b) showed no significant change in image quality using a TI of anything above. Fig 4c was acquired using a TI of 2800ms.

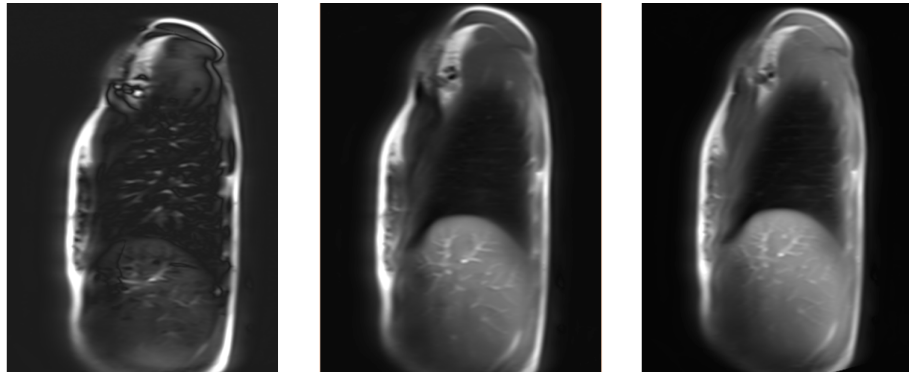


Figure 17: Lung images acquired using inversion times of 600ms, 700ms and 800ms respectively

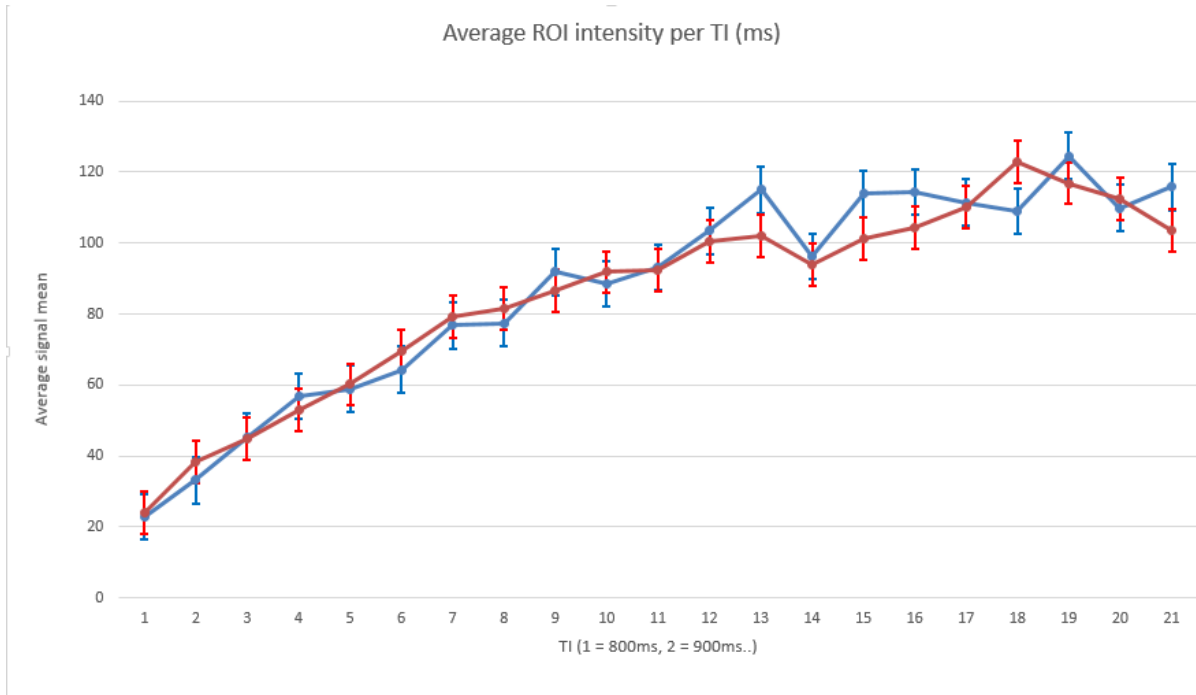


Figure 18: Plot showing average signal intensity of each tested inversion time in steps of 100ms, starting at 800ms.

6 Discussion

6.1 Analysis of 1.5T experiments

Without the availability of a non-selective inversion pulse, clear lung images with no blood signal proves hard to image. Some imaging systems such as our used SIEMENS scanners don't provide this option only having the slice selective inversion pulse. The slice inversion pulse does not provide any improvements in blood signal attenuation and is apparent in acquired image series.

All signal intensity relative to each voxel relates to a specific T1 relaxation time. By relying only on the rate of equilibration in determining SV, factors such as water vapour and dead space that alter the steady-state equilibrium (while remaining largely constant) can be ignored [14]. Another advantage for only measuring the rate of equilibration is identifying the difference in SV in subjects presenting identical ventilation-perfusion ratios; subjects with higher SV will have a faster rate of equilibration.

A plot of mean signal intensity at each breath was plotted shown on figure 11. As mentioned before, we expect to see clear changes in signal intensities when switching gas delivery

back and forth from air to oxygen. We expected our plot to resemble a similar trend shown on figure 2 where these fluctuations are clearly observed. Instead, our resulting plot presented random fluctuations regardless of oxygen delivery in mean signal intensities as we step through the image series. Overall signal change from air to oxygen were apparent where lower signal intensities were found in air breathing blocks and higher intensities in oxygen breathing blocks. The overall signal change observed does not provide confirmation on proper oxygen delivery, hence the thresholding method is introduced.

Performing data-analysis on blood spoiled images showed inaccurate results in both SV quantification and regional SV distribution. By introducing a thresholding method where nulling blood signals inside the lung ROI is made possible, accuracy and quality of analysis is improved.

6.1.1 Thresholding of blood

Due to the vascular nature of the lung, a non-selective inversion recovery pulse is required to null blood signal inside our ROI. As we are analyzing the lung relative to its signal intensities per voxel, noise such as blood appearing bright will give false data in our analysis. Using a slice-selective inversion pulse ($T_1=1000\text{ms}$) we could not null the blood in our acquired images. In a series of 220 images, around 15 images were available for use and the rest presented large amounts of noise in the region of interest. By concluding the necessity of a non-selective inversion pulse sequence, I aimed to find other ways of presenting reliable analysis of the images.

The non-selective inversion pulse aims to null all signals coming from cardiac movements during our breathold by inverting all magnetic dipoles. When we only use a slice-selective inversion recovery pulse, only one slice is inverted, therefore, blood signal from the other lung slices appear during image acquisition. For example, blood from other slices of lung that have not been inverted flow to the imaging slice from normal cardiac function. The slice-selective inversion recovery pulse nulls blood signals from only a single slice but due to the continuous flow of blood, non-inverted signals from the same heart cycle appear at the time of imaging.

Having blood signal appearing in our region of interest greatly reduces the accuracy of our results. Typically, the mean signal intensity inside the lungs from an image showing no blood noise range from 40 to 50. Images presenting signal from blood can range anywhere between 100 to 300. Although we can see relative changes in signal intensities between volunteers

breathing in air versus oxygen, the accuracy is far off and results look unreliable.

We expect to see a range of signals as we step through the air-oxygen cycle. When a volunteer is breathing in oxygen, signal intensities should be low around 40 to 50. Following inhalation of 100% oxygen, the signal intensity is expected to increase due to the increase in oxygen concentration inside the lungs. On average, signal intensities following inhalation of pure Oxygen are 15% - 20% higher than signals from air. Finding the mean signal intensity of the whole lung ROI including images with high blood signals showed to have major accuracy issues where signal intensity can range up to from 200%. Experimentally, this information provides no relevant data for further analysis as the signal-to-noise ratio too low. To overcome this problem, I tried different ways in finding the estimate mean signal intensity in the ROI when no blood signal is present.

Firstly, I placed a square ROI in the middle of our lung image and measured its mean signal intensity. Repeating this for all images in the series allowed me to see if any signal change was present when our volunteer is breathing air and oxygen. As mentioned before, we expect to see a lower intensity when breathing in air, and higher intensities when breathing oxygen. Plotting the mean signal intensity of each ROI in the image series, I saw the expected trend of the signal intensities ranging from low to high. Although the trend was very unreliable, it did provide information on our oxygen delivery working as it should. A further quality analysis was performed where any images presenting high blood signals (over 100) were discarded and taken out of our improved signal intensity graph using quality images. This provided us with a more observable and expected plot showing clear changes in signal variation from air to oxygen. As a large proportion of images were discarded (160+ images), this improved method is still not reliable nor accurate providing the need for a better analysis method.

6.1.2 Post-Threshold analysis

The last method I tried was to threshold the signals from blood out of our final analysis in attempt to find the true mean signal intensity of that ROI. By using MATLAB, I wrote a code that filters out signal coming from blood. An image showing no blood signal has an average intensity of 42. Choosing a threshold intensity equivalent or near the average signal intensity of blood would null bloods signal leaving the only relevant voxels for analysis. Testing with multiple threshold values, I concluded to use a threshold value of 90.

Performing our data analysis on the post-threshold image series showed a much better

and expected trend where signal intensities would fluctuate up and down as we step through our air – oxygen cycle (figure 14). We can see a clear increase in mean signal intensity of voxels increasing following inhalation of oxygen and a clear decrease following inhalation of air. The post-threshold results also decreased the average signal intensity value. In the data set before thresholding, mean signal intensities would range from 37 to over 70. In the post-threshold data set, the same image series ranged from 42 to under 60. The intensity signal range should fluctuate around 15% to 20%. Averaging mean signal intensities at each air and oxygen cycle, I calculated the relative % signal change for both pre/post-threshold data sets. The pre-threshold data set showed an % signal change of 40% between each air – oxygen cycles. For the post-threshold data set, the average % signal change was found to be 18%.

From these findings, we can conclude most analysis errors was the result of blood signals showing in our acquired images series.

6.2 Shared Data analysis

6.2.1 Quantifying limitations in our experiment

Observable trends on regional SV distribution is seen on the clean image sets where SV is higher at the bottom of lung represented by more warm colours on the SV map (figure 15A). This is expected as gravity plays a role in gas exchange. Lower lung heights are under more force compared to higher heights of lung due to being under force from organs its supporting and its lower center of gravity. The increase in pressure slightly increases the efficiency of gas exchange as gas high pressures cause larger pressure gradients, hence more exchange of air. SV maps of the spoiled image series show no observable trend in regional SV distribution and fail to provide useful information. This is expected and further validates the quantification of errors coming mainly from blood. Finding the height plots of the two SVI maps (figure 16A/B) show a vertical SV gradient as we step down in lung heights by 1cm.

The drastic change in plot profiles is explained from increased signals coming from the lung ROI. Due to signal coming from blood, measurement of average SV units will largely fluctuate. In a given centimeter height of lung, true SV signal (low 50s) may exist among false signal initiated by blood (high 300s). The large difference in same lung heights cause these unorthodox spikes to appear in the height plot. We saw consistent appearances of these spikes in our final analysis with different image sets, both shared and obtained.

The spikes on figure 16b shown by dashed lines represent the standard deviation of SV

within that height of lung. When there is a high influence of signal intensity from the blood signal, this spike would be larger causing an increase in signal variation. With the increase in signal variation, the standard deviation of SV also increases which is seen by the dashed lines situated in the negative axis.

From these results paired with the thresholding results, the effect of blood in spoiling our data analysis became more apparent.

6.3 Analysis of 3T experiments

The 3T MRI scanner showed no improvements in image quality. In a typical 3T scanner, blood can be signaled out using an inversion time of 1350ms [19]. Experimenting with multiple inversion times, blood signal consistently showed throughout. Another improved experiment using increased range of inversion times was performed, starting at 600ms then finishing at 2800ms in intervals of 100ms. This was repeated for both air and oxygen and 8 images were scanned at each TI. A total of 368 images were scanned. However, inversion times of 600ms and 700ms produced poor quality images and were discarded from further analysis. Like before, scanning the lungs using the chosen inversion times did not null the blood as it consistently showed in most images. Varying inversion times only changed the brightness of the image where a higher inversion time, shows a brighter image.

Further analysis on the 3T images were carried out by measuring the mean signal intensity of an ROI that evades all blood signal. Using an oval ROI, I chose a spot that had the greatest number of pixels but also having the least amount of blood signal. As blood signals appear roughly in the exact spot at each image, the chosen ROI consistently avoided large fluctuations in signal intensity from the influence of blood. As the goal of this experiment using multiple inversion times was finding an inversion time nullifying blood, analysis of oxygen delivery per air-oxygen cycle was not possible.

In attempt to find further information from our experiment, I calculated the average mean signal at each inversion time for both air and oxygen. Images following inhalation of 100% oxygen are expected to have higher signal intensities compared to images following inhalation of air. By plotting the average mean signal change, stepping through each inversion time, we expect to see a steady increase in signal intensity at each TI with oxygen always having a higher intensity than air. The result was a plot showing an increase in mean signal with increasing inversion times, however failed to display oxygen signal intensities always being

higher than air. Signal intensities above inversion times of 1900ms showed mostly air having highest signal intensities compared to oxygen. This is incorrect and remains unreliable for further discussion.

7 Conclusion

This project discussed the use of Oxygen-enhanced MRI and how it can be applied to obtain clinical measurements inside the lung providing comparable results with current gold standards [15]. Using both 1.5T and 3T scanning systems we were able to closely follow Sa et al's methods and produce inaccurate image series presenting information of SV. Resulting images had noise present due to the unavailability of the non-selective inversion pulse, however, efforts have been made to bypass this limitation such as thresholding blood out of acquired lung images. As a result, we were able to confirm irregular graph trends and values relating to SV through prewritten MATLAB codes was the result of unwanted blood signals in the imaged lung.

8 Reference

- [1] World Health Organization. The top 10 causes of death. Available at: <http://www.who.int/mediacentre/> (Accessed 14 March)
- [2] World Health Organization. World Health Statistics. 2008: <http://www.who.int/whosis/whostat/2008.html>
- [3] The Asthma Foundation. Burden of Respiratory Disease. Available at: <http://asthmafoundation.org/burden-of-respiratory-disease.html> (Accessed 10 March).
- [4] Chen Q, Jakob PM, Griswold MA, Levin DL, Hatabu H, Edelman RR. Oxygen enhanced MR ventilation imaging of the lung. MAGMA 7: 153–161, 1998. [5]
- [6] Edelman RR, Hatabu H, Tadamura E, Li W, Prasad PV. Noninvasive assessment of regional ventilation in the human lung using oxygen- enhanced magnetic resonance imaging. Nat Med 2: 1236–1239, 1996.
- [7] Hickam JB, Blair E, Frayser R. An open-circuit helium method for measuring functional residual capacity and defective intrapulmonary gas mixing. J Clin Invest 33: 1277–1286, 1954.
- [8] Lewis SM, Evans JW, Jalowayski AA. Continuous distributions of specific ventilation recovered from inert gas washout. J Appl Physiol 44: 416–423, 1978.
- [9] Ley-Zaporozhan J, Ley S, Kauczor HU. Morphological and functional imaging in COPD with CT and MRI: present and future. Eur Radiol 2008, 18:510-521.
- [10] Ley-Zaporozhan J, Ley S, Kauczor HU. Proton MRI in COPD. COPD 2007, 4:55-65.
- [11] Mai VM, Tutton S, Prasad PV, Chen Q, Li W, Chen C, Liu B, Polzin J, Kurucay S, Edelman RR. Computing oxygen-enhanced ventilation maps using correlation analysis. Magn Reson Med 49: 591–594, 2003.
- [12] Milic-Emili J, Henderson JA, Dolovich MB, Trop D, Kaneko K. Regional distribution of inspired gas in the lung. J Appl Physiol 21: 749–759, 1966.
- [13] Miller GW, Mugler JP, 3rd, Sa RC, Altes TA, Prisk GK, Hopkins SR. Advances in

functional and structural imaging of the human lung using proton MRI. NMR Biomed 2014, 27:1542-1556.

[14] Sá RC, Cronin MV, Cortney Henderson A, Holverda S, Theilmann RJ, Arai TJ, Dubowitz DJ, Hopkins SR, Buxton RB, Kim Prisk G. Vertical distribution of specific ventilation in normal supine humans measured by oxygen-enhanced proton MRI. J Appl Physiol 109: 1950– 1959, 2010.

[15] Sá, Rui Carlos, et al. "Validating the distribution of specific ventilation in healthy humans measured using proton MR imaging." Journal of Applied Physiology 116.8 (2014): 1048-1056.

[16] Mead, Jere, and James L. Whittenberger. "Physical properties of human lungs measured during spontaneous respiration." Journal of Applied Physiology 5.12 (1953): 779-796.

[17] Cook, Fredrick Roscoe, et al. "Rapid Prototyping of Inspired Gas Delivery System for Pulmonary MRI Research." 3D printing and additive manufacturing 2.4 (2015): 196-203.

[18] Bushong, Stewart C., and Geoffrey Clarke. Magnetic resonance imaging: physical and biological principles. Elsevier Health Sciences, 2014.

[19] Jacobs, Michael. "Totally Accessible MRI: A User's Guide to Principles, Technology, and Applications." Medical Physics 35.11 (2008): 5198-5198.

[20] Basic Principles of MR: <https://radiologykey.com/basic-principles-of-mri/>